Neuroradiology (1990) 32: 416–420

Neuro radiology

Sodium-23 magnetic resonance brain imaging*

S. S. Winkler

Radiology Service, William S. Middleton Memorial Veterans Hospital and Department of Radiology, University of Wisconsin Medical School, Madison, Wisconsin, USA

Summary. This is a review of recent work in ^{23}Na MR imaging. The main emphasis of recent papers has been pulse sequences that, with appropriate postprocessing, give images of the fast, slow, and intermediate components of T2 decay. The assignment of compartmental designation to the T2 component remains a problem except for homogeneous structures easily identifiable anatomically (ventricles, superior sagittal sinus, globe of the eye). Compartmental distribution of sodium is described. The predominance of the interstitial and plasma compartment, the invisibility of part of the intracellular sodium, and the difficulty in imaging the very fast T2 component of visible intracellular sodium make the usual Na spin-echo image essentially an image of the interstitial and plasma space. Use of super paramagnetic iron oxide coupled to dextran as a contrast medium may help to identify the plasma compartment. Because the usual Na MR images are essentially interstitial and plasma images, our own interest is in observing functional changes in these compartments. Another proposed application is the detection of the very fast T2 component in brain tumors to aid in defining tumor grade and extent.

Key words: Brain – Sodium – Magnetic resonance imaging

Sodium-23, which comprises virtually 100% of naturally occurring sodium, is the only nucleus other than the proton that can be imaged in its natural abundance. The average concentration of Na + ions in brain is 1/2000 that of protons, and the sensitivity of the ^{23}Na nucleus is about one tenth that of the proton. Unlike protons, which have a nuclear spin of 1/2 (dipolar relaxation), Na + has a spin of 3/2 (quadrupolar relaxation). Sodium can have three transition and two T2 relaxation rates, a short component of about 0.7–3.0 ms and a long component of 16–60 ms [1–3]. Proton and ^{23}Na MR characteristics are compared in Table 1.

* Supported in part by the Department of Veterans Affairs Medical Research Service

Because of quadrupolar relaxation and biexponential T2 decay, a portion of sodium in biological tissue – especially the intracellular sodium – is invisible even to NMR spectroscopy. Although exact visibility data for the living brain are not available, several authors have suggested, on the basis of data from other systems, that as much as 60% of the intracellular sodium may not be visible to MR, whereas almost all of the extracellular portion is believed to be fully visible [2, 3]. Other work suggests that half of the visible portion of intracellular sodium may be difficult to image because of very rapid T2 decay [4].

Previous work has emphasized applications that grossly increase the extracellular compartment (vasogenic edema), cause loss of the intracellular compartment (infarction), or cause increase in intracellular sodium (tumor, cytotoxic edema) [5, 6]. It is clear that Na MR imaging applications must provide information not available on proton MR imaging. Thus the work of Hilal et al. suggests that Na MRI provides information on the extent and grade of supratentorial tumors not available from conventional proton MRI. Our approach is to look at the normal distribution of sodium and at how ^{23}Na signal and T2 relaxation may be coupled to the well studied factors cerebral blood volume and interstitial volume, to reveal subtle abnormalities not evident on proton MRI.

To understand Na MRI one must first consider the compartmental distribution of sodium. In other words, if all compartments were equally represented on an Na MR image, what would we see? Since we know that the regional T2 decay of sodium is heterogeneous and multi-

Table 1. Nuclear properties and sensitivities of ^{1}H and ^{23}Na in the brain[a]

Nucleus	Spin	Gyromagnetic ratio ($\gamma/2\pi$)	Frequency at 1.5 T (MHz)	Relative MR sensitivity[b]	Normal regional brain concentrations	Relative sensitivity[c]
^{1}H	1/2	43 MHz/T	64	1	100,000 mM	1
^{23}Na	3/2	11 MHz/T	17	0.13	25–145 mM	6×10^{-5}

[a] Adapted from Perman et al. [3]
[b] At constant field for equal number of nuclei
[c] At constant field and normal physiological concentration

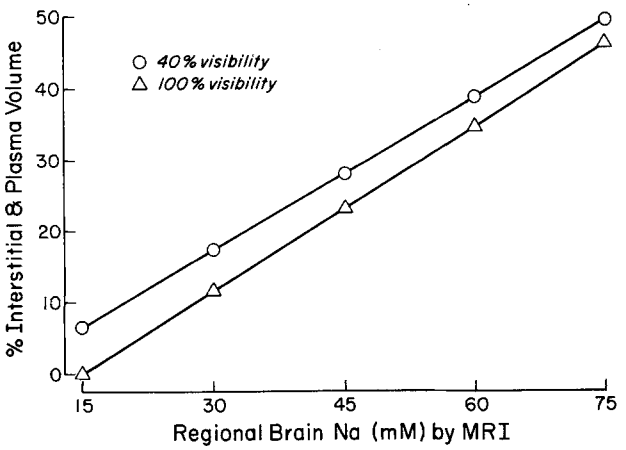

Fig. 1. Representation of eq. (1) for 100% and 40% intracellular Na MR "visibility". Comparison of the two lines shows the difference in computation of extracellular and plasma volume if the intracellular "invisible" sodium is taken into account. Note that the effect of sodium invisibility becomes less in regions with higher sodium levels because the proportion of total sodium that is intracellular is relatively small in these regions

exponential, we must consider imaging strategies that will selectively differentiate these compartments. We will show our initial approach to this problem.

Compartmental distribution of ^{23}Na in normal brain

The relationship of regional brain sodium concentration (rCNa) to its compartmental distribution is as follows. Let:

f = fraction of brain comprising combined plasma and interstitial compartment;

c = Na concentration in combined plasma and interstitial compartment;

d = intracellular Na concentration.

Then $c(f) + d(1-f) = \text{rCNa}$, or

$$f = (\text{rCNa}-d)/(c-d) \qquad (1)$$

Since the sodium concentrations in the combined plasma and interstitial compartments are known and identical, and since the average intracellular concentration can probably be assumed constant throughout the normal brain, variations in rCNa are proportional to the size of the regional combined plasma and interstitial compartments. If we let $c = 145$ mM and $d = 15$ mM, then eq. (1) becomes $f = (\text{rCNa}-15)/130$ (displayed in Fig. 1 for 100% and 40% intracellular sodium visibility).

Figure 1 shows that whether or not we take into account the invisibility of intracellular sodium, the Na MRI signal is largely dependent on the size of the combined interstitial and vascular space – especially if we look at cortex, which according to direct measurements has a sodium concentration between 45 and 53 mM [7, 8]. By using published measurements of compartmental size [9, 10], it is possible to calculate the expected contribution of each compartment to the regional sodium (Tables 2, 3). For measuring the plasma space, we use the values obtained by the anatomical studies of Weiss et al. [11] rather than those obtained from nuclear tracer studies, which are lower by about 50% [12]. The reasons are as follows.

1. Weiss et al. have found that at any instant, only about 50% of cortical capillaries are in use, the rest being available for recruitment. This explains the lower values found in nuclear tracer studies, which would be expected to visualize only those vessels in use.

2. By using the data of Weiss et al., we arrive at a value for cortical sodium that is in good agreement with experimental determination; but if we use the nuclear tracer value, we arrive at a value that is about 25% lower than expected (Tables 2, 3).

Tables 2 and 3 show that, while most of the brain volume is cellular, the sodium is predominantly in the plasma and interstitial compartments. The plasma compartment, which comprises only 5% of the total cortical volume, contains 20% of cortical sodium by Na MRI. In the usual spin-echo sequence we obtain images that selectively image the interstitial and plasma space. Na MRI sees the naturally abundant ^{23}Na in both recruited and unrecruited vessels, because unrecruited vessels are not empty or collapsed and can only be distinguished in animal studies by the presence of indicator dye introduced just before sacrifice [11]. The unrecruited portion of the vascular space is spatially heterogeneous and not readily accessible to nuclear tracer measurement. Thus ^{23}Na MRI might be sensitive to functional changes affecting the vascular and interstitial compartments.

Table 2. Compartmental distribution of sodium in cerebral cortex*

Compartment	Fraction of cortex volume (1)	Na concentration (mM) (2)	Contribution to total cortex Na [mM; (1) × (2)] (3)	Fraction of total cortex Na (3) ÷ 47.4	Fraction of total MR-visible ^{23}Na[a]
Intracellular	0.75	15	11.2	0.24	0.11
Interstitial	0.20	145	29	0.61	0.71
Plasma[b]	0.05	145	7.2	0.15	0.18
Total	1.00	–	47.4	1.00	1.00

* See footnotes to Table 3

Table 3. Compartmental distribution of sodium in cerebral white matter

Compartment	Fraction of white matter volume (1)	Na concentration (mM) (2)	Contribution to total Na [mM; (1) × (2)] (3)	Fraction of total Na (3) ÷ 25.4	Fraction of total MR-visible ^{23}Na[a]
Intracellular	0.92	15	13.8	0.54	0.32
Interstitial	0.05	145	7.3	0.29	0.43
Plasma[b]	0.03	145	4.3	0.17	0.25
Total	1.00	–	25.4	1.00	1.00

[a] Assuming only 40% of intracellular Na is visible to MRI and interstitial and plasma Na is totally visible

[b] Calculated at large vessel hematocrit of 45 and corrected for cerebral hematocrit (0.75 × large vessel hematocrit) [12]

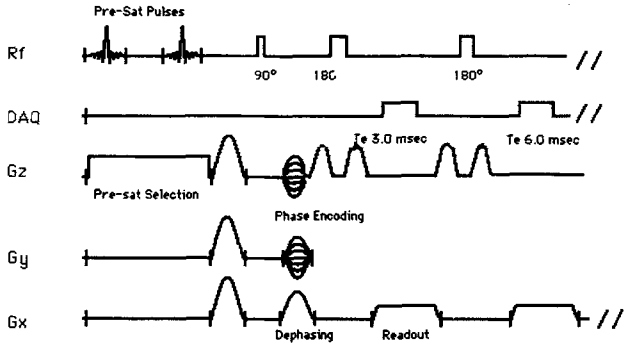

Fig. 2. 3-D presaturation multispin echo pulse sequence using nonselective 180° pulses for echo formation. Phase encoding is done in the y (128 steps) and z (16 steps) directions; frequency encoding is done in the x direction (128 steps)

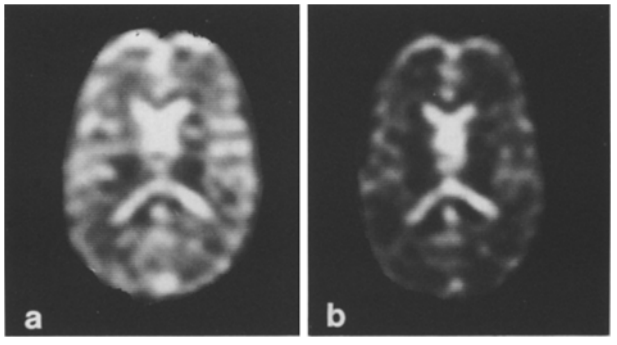

Fig. 3. **a** First echo of spin echo sequence. **b** Second echo. $T_E = 3$ ms, $T_R = 98$ ms, in-plane resolution = 0.7 × 0.7 cm, slice thickness = 1 cm

Technical factors

The following are important technical considerations for Na MRI imaging strategies.

Static magnetic field. Signal-to-noise ratio is approximately proportional to static magnetic field. Since we are dealing with a low signal-to-noise ratio, higher field strength systems are advantageous. We are using a 1.5-Tesla GE Signa system.

Imaging time. All other factors being equal, signal-to-noise ratio is proportional to the square root of the imaging time. The range that we find practical is 17–34 min.

Pulse sequence. The pulse sequence we are using is shown in Fig. 2 [13]. In a spin echo data acquisition protocol, the observed signal intensity decreases as

$I = I_0 \exp(-T_E/t_2)$

where I is the signal induced in the receiver coil, T_E is the echo time, and t_2 is the spin-spin relaxation time. For in vivo sodium, the relaxation times are on the order of 0.7–60 ms. To maximize the acquired signal from the brain, to minimize the amount of undetected sodium, and especially to obtain regional T2 information, the echo time should be as short as possible even though there is some sacrifice of spatial resolution. We are using a T_E of 3 ms and T_R of 100 ms. T_E's shorter than 3 ms are not practical with a spin echo sequence. Because about half of the visible intracellular sodium component may have T2 ≤ 2 ms [4], we are probably seeing very little intracellular sodium on our images. This is actually advantageous for us because our interest is in the interstitial and plasma components. On the other hand, Hilal et al., who are primarily interested in intracellular sodium, use an image formed from the initial FID signal to include the very fast T2 components [5, 14].

Image reconstruction. One method of increasing the signal-to-noise ratio for an imaging sequence is to acquire the signal from a larger total volume. This is possible with a pulse protocol that excites a volume of spins, phase-encodes in both the y and z directions, and frequency-encodes in the x direction.

Post-processing of images

In previous work we found that the T2 of cortex is 8–14 ms and that of CSF is about 50 ms; that of blood is intermediate between the two [15]. Yet on a single image, these tissues cannot be distinguished – they all have high signals (Fig. 3 a). This limitation is especially serious in the region of the cortex where CSF and gray matter are in proximity. We can overcome the limitation by using two or more images of a multiple spin echo sequence and obtaining processed images that distinguish the various tissues by their different T2 decays. Figure 3 a and b show the first and second echoes in a multiple spin echo sequence (T_E 3 ms, T_R 98 ms). The images in Fig. 4 are processed images derived from the two images in Fig. 3. The top row shows all voxels in Fig. 3 a that have decayed more than a given fraction of the signal between Fig. 3 a and b. The bottom row shows all voxels that have decayed less than a given fraction. As we go from left to right on the top row, we see sodium tissues of ever shorter T2. The separation of cortex and CSF on the basis of T2 is clear on these images. The superior sagittal sinus, which is initially in the faster row, is seen switching to the slower row between 0.7 and 0.65 *(arrows)*. We are helped by being able to identify these structures anatomically. The question to be answered is, what other compartments or tissues are represented? – e.g., will we be able to distinguish capillary blood from interstitial fluid?

Our method of using fractional threshold seems preferable to calculating T2 or 1/T2 images [15]. It is possible also to form narrower windows of T2 values. In this example we are looking at only two echoes. We are regularly able to obtain four equally spaced echoes, and by applying the same analysis to the two succeeding echo pairs we can obtain some further insight into whether T2 decay in a given voxel is multiexponential or monoexponential and can obtain more accurate T2 values.

The method of Hilal et al. [5, 14], while different in details, employs the same principles: pulse sequence sensitive to both fast and slow T2 and postprocessing to selectively image fast and slow regions. Their method has some ingenious features: using an initial FID signal image that is assumed to represent total sodium; assigning extracellular sodium to the late echoes; extrapolating back to the FID image; and using the CSF as a standard for extracellular sodium. They then post-process images that are desig-

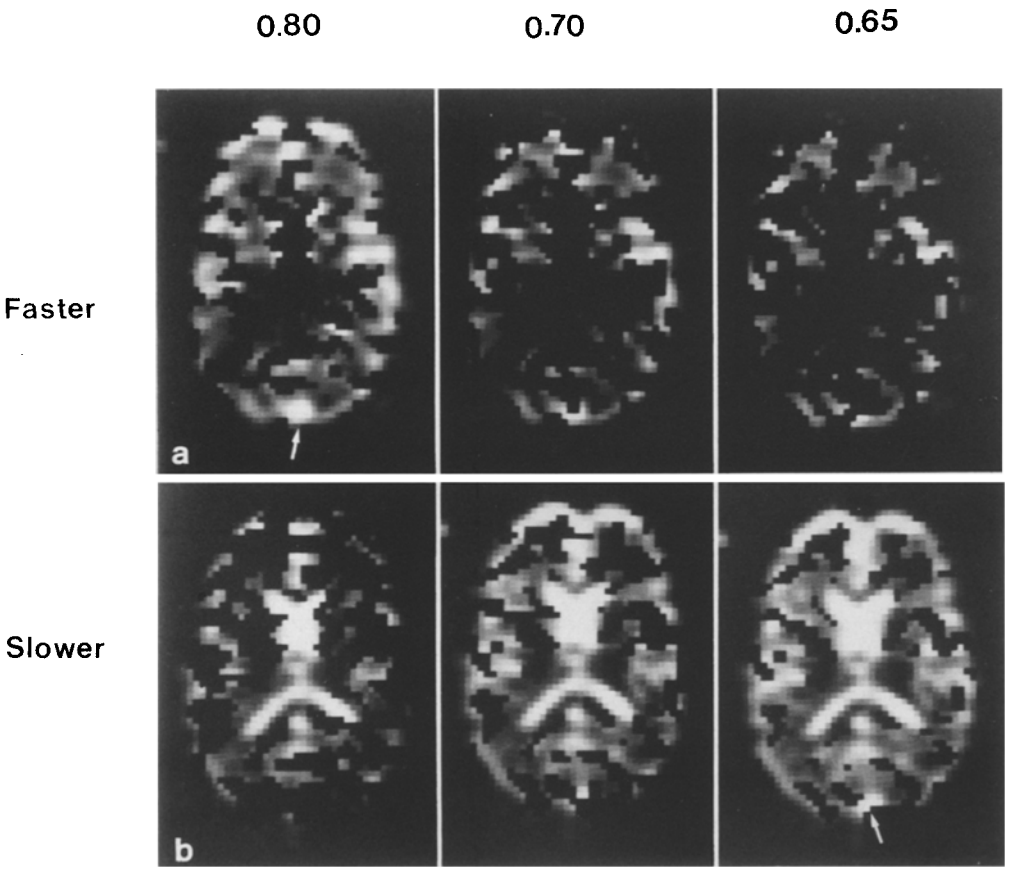

Fig. 4a, b. Postprocessing of images of Fig. 3. Each vertical pair (**a, b**) is a complementary pair in which voxels are separated on the basis of whether the signal decays faster or slower than the given fraction (0.80, 0.70, 0.65) of the initial signal. If recombined each complementary pair would give the first echo image (Fig. 3a). The superior sagittal sinus *(arrows)* moves from faster to slower row between 0.70 and 0.65

nated intracellular sodium concentration image, extracellular sodium concentration image, etc. In a recent publication [16] the authors acknowledge that their method employs several unvalidated assumptions but stress its heuristic value in predicting tumor grade and extent. While it seems likely that the various regional T2 values identified on a post-processed image have some relationship to the physiologic sodium compartments, this relationship needs to be verified.

Contrast agents

Paramagnetic compounds of the rare earth metal dysprosium have been used as a shift reagent for sodium spectroscopy, and can be used to obtain separate spectra for intracellular and extracellular sodium in cell preparations in which the dysprosium is confined to the extracellular space [17]. It is doubtful, however, that shift reagents have any role in sodium imaging even if they can be confined to the vascular space and be safely administered to the intact animal. A more promising approach for imaging is the use of superparamagnetic contrast agents confined to the vascular space. Summer et al. [18] have shown that magnetite (Fe_3O_4, containing Fe II and 2Fe III) coupled to dextran, when administered intravenously to mice, will eliminate the signal originating in the blood pool through shortening of T2 for about one hour. Bogdan et al. [19] have used this method to eliminate the vascular sodium signal in order to obtain an accurate measure of extravascular water in the rat model of pulmonary edema. We are planning to apply the same method to determine how much of the cortical sodium signal is from the plasma compartment in the experimental animal. These compounds are currently under investigation for human use to aid in diagnosis of liver neoplasms, and thus their application to human Na MRI is conceivable [20].

Concluding comment

The images in the "faster" row of Fig. 4 resemble a cerebral blood flow or blood volume image as seen on PET or xenon-CT. It is the personal opinion of this reviewer that this appearance is not accident, and that just as brain research of the past several decades has demonstrated close coupling of regional brain metabolism, regional capillary volume, and regional brain blood flow and volume, these factors also will be found to couple to regional sodium signal and T2, and it is here that Na MRI will find its most important clinical application.

References

1. Hilal SK, Maudsley AA, Simon HE, Perman WH, Bonn J, Mawad ME, Silver AJ, Ganti SR, Sane P, Chien IC (1983) In-vivo NMR imaging of tissue sodium in the intact cat before and after acute cerebral stroke. AJNR 4: 245–249

2. Hilal SK, Maudsley AA, Ra JB, Simon HE, Roschmann P, Wittekoek S, Cho ZH, Mun IK (1985) In vivo NMR imaging of sodium-23 in the human head. J Comput Assist Tomogr 9: 1–7
3. Perman WH, Turski P, Houston L, Glover GH, Hayes CE (1986) Methodology of in vivo human sodium NMR imaging at 1.5 Tesla. Radiology 160: 811–820
4. Burstein D, Fossel ET (1987) Intracellular sodium and lithium NMR relaxation times in the perfused frog heart. Magn Reson Med 4: 261–273
5. Hilal SK, Ra JB, Oh CH, Mun IK, Einstein SG, Roschmann P (1987) Sodium imaging. In: Stark DD, Bradley WG (eds) Magnetic resonance imaging. Mosby, St. Louis, pp 715–731
6. Turski PA, Perman WH, Houston L, Winkler SS (1988) Clinical and experimental sodium magnetic resonance imaging. Radiol Clin North Am 26: 861–871
7. Siesjö BK, Deshpande JK (1987) Electrolyte shifts between brain and plasma in hypoglycemic coma. J Cereb Blood Flow Metab 7: 789–793
8. Young W, Rappaport ZH, Chalif DH, Flamm ES (1987) Regional brain sodium, potassium, and water changes in the rat middle cerebral artery occlusion model of ischemia. Stroke 18: 751–759
9. Levin VA, Fenstermacher JD, Patlak CS (1970) Sucrose and inulin space measurements of the cerebral cortex in four mammalian species. Am J Physiol 219: 1528–1533
10. Pelligrino DA, Musch TI, Dempsey JA (1981) Interregional differences in brain intracellular pH and water compartmentation during acute normoxic and hypoxic hypocapnia in the anesthetized dog. Brain Res 214: 387–404
11. Weiss HR, Buchweitz E, Murtha TJ, Auletta M (1982) Quantitative regional determination of morphometric indices of the total and perfused capillary network in the rat brain. Circ Res 51: 494–503
12. Sakai AK, Nakazawa K, Tazaki Y, Ishii K, Hino H, Igarashi H, Kanda K (1985) Regional cerebral blood volume and hematocrit measured in normal human volunteers by single photon emission computed tomography. J Cereb Blood Flow Metab 5: 207–213
13. Perman WH, Thomasson DM, Bernstein MA, Turski P (1989) Multiple short echo 2.5 ms quantitation of in vivo sodium T2 relaxation. Magn Reson Med 9: 153–160
14. Ra JB, Hilal SK, Oh CH (1989) An algorithm for magnetic resonance imaging of the short T2 fraction of sodium using the FID signal. J Comput Assist Tomogr 13: 1–8
15. Winkler SS, Thomasson DM, Sherwood K, Perman WH (1989) Regional T_2 and sodium concentration estimates in the normal human brain by sodium-23 MRI at 1.5 T. J Comput Assist Tomogr 13: 561–566
16. Hilal SK, Oh CH, Mun IK, Johnson G (1989) Grading of gliomas by sodium MRI (abstract). Proc Soc Magn Reson Med, Berkeley, CA, p 83
17. Gupta RK, Gupta P (1982) Direct observation of resolved resonances from intra and extracellular sodium-23 in NMR studies of intact cells and tissues using dysprosium (III) tripolyphosphate as paramagnetic shift reagent. J Magn Reson 4: 344–350
18. Summers RM, Joseph PM, Renshaw PF, Kundel HL (1988) Dextran magnetite: a contrast agent for sodium-23 MRI. Magn Reson Med 8: 427–439
19. Bogdan A, Lancaster L, Kundel H (1989) Sodium MRI of extravascular lung water using coated magnetite particles (abstract). Proc Soc Magn Reson Med, Berkeley, CA, p 663
20. Stark DD, Weissleder R, Elizondo G, Hahn PF, Saini S, Todd LE, Wittenberg J, Ferrucci JT (1988) Superparamagnetic iron oxide: clinical application as a contrast agent for MR imaging of the liver. Radiology 168: 297–301

S. S. Winkler, M. D.
Radiology Service
William S. Middleton Memorial Veterans Hospital
2500 Overlook Terrace
Madison, Wisconsin 53705
USA